Journal of Constructional Steel Research 66 (2010) 139–149

Contents lists available at ScienceDirect

Journal of Constructional Steel Research

journal homepage: www.elsevier.com/locate/jcsr

Local buckling restraint condition for core plates in buckling restrained braces

T. Takeuchi [a,*], J.F. Hajjar [b,1], R. Matsui [a,2], K. Nishimoto [c,3], I.D. Aiken [d,4]

[a] Department of Architecture and Building Engineering, Tokyo Institute of Technology, Tokyo, Japan
[b] Department of Civil and Environmental Engineering, University of Illinois at Urbana-Champaign, IL, USA
[c] Building Construction & Steel Structure Division, Nippon Steel Engineering Co. Ltd., Tokyo, Japan
[d] Seismic Isolation Engineering, Inc., Emeryville, CA, USA

ARTICLE INFO

Article history:
Received 8 July 2009
Accepted 5 September 2009

Keywords:
Steel structures
Seismic
Buckling restrained brace
Local buckling failure
Restraint performance

ABSTRACT

Buckling Restrained Braces (BRBs) are commonly used as bracing elements in seismic zones. A key limit state governing BRB design is to prevent flexural buckling. However, when the wall thickness of the steel tube restrainer is relatively small compared to the cross-section of the core plate, the restraint conditions against the local buckling of the core plate can be critical for the stability and strength of the BRB. In this study, cyclic loading tests and numerical analyses of BRBs were carried out using various tube restrainer configurations to investigate the influence of local buckling of the restrainer on BRB strength and ductility.

1. Introduction

Buckling restrained braces (BRBs) comprise a steel core plate restrained by a mortar filled tube or other mechanism that prevents overall flexural buckling of the core plate. BRBs were developed for practice in the 1980's in Japan [1], and have been employed in more than two hundred buildings as ductile bracing members or hysteresis dampers. Numerous researchers have conducted experiments and numerical analyses on BRBs for incorporation into seismic force resisting systems. Qiang [2] has investigated the use of BRBs for practical applications for buildings in Asia. Clark et al. [3] suggested a design procedure for buildings incorporating BRBs. Black et al. [4,5] carried out component testing of BRBs and modeled a hysteresis curve, comparing to test results. Sabelli et al. [6] reported seismic demands on BRBs via seismic response analyses of BRB frames, and Fahnestock et al. [7,8] carried out numerical analyses and pseudodynamic experiments of large-scale BRB frames in the US. Through these studies, the conditions for the BRB to obtain a stable hysteresis can be classified as follows.

(a) When an axial force is applied to the core plate, the restrainer should have a sufficient stiffness to prevent overall flexural buckling of the BRB.
(b) A core plate section expands when it is compressed into the plastic range; thus, a certain amount of clearance to avoid the friction between the core plate and the restrainer must be provided to prevent the core plate from bearing directly to the restrainer, leading to inelastic buckling through transfer of the axial force to the restrainer.
(c) Given a clearance between the core plate and the external restrainer, the core plate buckles slightly, and perpendicular force components are produced at each peak of the buckling wave. The walls of the restrainer should possess sufficient stiffness and strength to restrain the core plate.
(d) The connections at both ends of the BRB must have sufficient stiffness and strength for the BRB to maintain stable performance under the expected maximum force and deformation.
(e) The effective buckling length for designing the BRB should be determined by considering the stiffness of the connections at both ends.

The properties of the BRB restrainer were discussed by Watanabe et al. [1], who indicated that the core plate yield force needs to be smaller than the elastic flexural buckling strength of the restrainer to prevent overall flexural buckling of the BRB [item

* Corresponding address: Tokyo Institute of Technology, M1-29, 2-12-1 Ookayama, Meguro-ku, Tokyo, 152–8550, Japan. Tel.: +81 3 5734 3165; fax: +81 3 5734 3165.
E-mail addresses: ttoru@arch.titech.ac.jp (T. Takeuchi), jfhajjar@illinois.edu (J.F. Hajjar), matsui.r.aa@m.titech.ac.jp (R. Matsui), nishimoto.kohji1@eng.nsc.co.jp (K. Nishimoto), ida@siecorp.com (I.D. Aiken).
[1] University of Illinois at Urbana-Champaign, 2129b Newmark Civil Engineering Laboratory, MC-250 North Mathews Avenue, Urbana, IL 61801-2352, USA. Tel.: +1 217 244 4027; fax: +1 217 265 8040.
[2] Tokyo Institute of Technology, M1-29, 2-12-1 Ookayama, Meguro-ku, Tokyo, 152–8550, Japan. Tel.: +81 3 5734 3165; fax: +81 3 5734 3165.
[3] Nippon Steel Engineering Co. Ltd., 6-3, Otemachi 2-chome, Chiyoda-ku, Tokyo 100-8071, Japan. Tel.: +81 3 3275 5114; fax: +81 3 3275 5978.
[4] Seismic Isolation Engineering, 1144 65th St., Unit D Emeryville 94608-1053, CA, USA. Tel.: +1 510 774 5818; fax: +1 510 595 7499.

0143-974X/$ – see front matter © 2009 Elsevier Ltd. All rights reserved.
doi:10.1016/j.jcsr.2009.09.002

Notations

A_c the section area of the core plate
A_e the cross-section area of the core plate elastic zone
B_c the width of the core plate
B_r the width of the restrainer wall
C_1 and C_2 the material parameters calibrated to tension coupon tests
E the elastic modulus of the core plate
E_{tc} the tangent modulus of the core plate
E_{tr} the tangent modulus of the restraint tube
I_c the moment of inertia of the core plate
i_c the radius of gyration of the core plate
I_r the moment of inertia of the restrainer wall per unit length
L_p the length of the plastic zone of the core plate
l_p the length of the local buckling wave of the core plate
M_p the plastic hinge moment of the restrainer wall
P_c the core plate axial force
P_{crl} the local buckling force of the core plate by using of the spring coefficient
P_{cy} the yield axial force of the core plate
P_{lb} the local buckling failure force of the core plate
P_r the perpendicular force of the core plate
P_{rlb} the ultimate perpendicular force of the core plate
s the clearance between the core plate and the restrainer
t_c the thickness of the core plate
t_r the thickness of the restraint tube
β_r the spring coefficient of the restraint tube per unit length along the axis
δ_c the displacement of the core plate
δ_g the extensometer displacement
ε_c the strain of the plastic zone of the core plate
ε_{pl} the plastic strain
ε_t the maximum tensile strain of the core plate
γ the local buckling failure index
ν_p the plastic Poisson's ratio
σ_{ys} the yield surface stress for isotropic hardening
$\sigma|_{ys}$ the yield surface stress at zero plastic strain
σ_{pl} the backstress for kinematic hardening
σ_{cy} the yield stress of the core plate
σ_{cr} the buckling stress by using $\bar{\lambda}$
α the hardening ratio of strength after yielding

(a)]. The appropriate conditions for clearance between the core plate and the restrainer [item (b)] were also discussed by Watanabe et al. [1] for a core plate within a rectangular steel tube restrainer. The conditions for a circular core tube with an outer circular tube restrainer were discussed similarly by Takeuchi et al. [9]. In [1], the condition of core plate local buckling [item (c)] was studied by using an elastic spring for the in-filled mortar, and it was concluded that there is only a small risk for local buckling failure in typical BRBs. The effect of the BRB connection stiffness [item (d)] was researched by Takeuchi et al. [10], Tsai et al. [11], and Kinoshita et al. [12], and the effective buckling load considering the stiffness of the connections of BRBs was researched by Tembata et al. [13] and Kinoshita et al. [14] [item (e)]. For the conditions in item (c), however, it has been reported that there are risks of local buckling failure where the wall thickness of the restrainer is relatively small compared to the cross-sectional area of the core plate [15]. In such a case, the core plate buckles about the strong axis, since neither the restrainer nor the thin layer of material between the wall of the restrainer and the core plate are able to prevent the local buckling, as shown in Fig. 1, and such failure can lead to overall buckling due to the additional eccentricity of the core plate.

In this study, BRBs with rectangular and circular steel tube restrainers with various tube thickness ratios are subjected to monotonic and cyclic loading, and the behavior of local buckling failures in the core plate and resultant deformations in the restrainer are investigated using both the experimental results and corroborating computational simulations. A proposal is then made for the criteria necessary to prevent this type of local failure mode in mortar-filled BRBs.

2. Buckling conditions using elasto-plastic spring support

When the effect of mortar between the edge of the core plate and the restrainer wall is negligible, local buckling failure as shown in Fig. 1(a) may be modeled by the core plate being supported by double steel plates at the top and bottom in the direction of the strong axis, as shown in Fig. 1(b) and (c).

The boundary condition at the corner of the restrainer wall is regarded as rigid, because the restrainer is filled with mortar. The spring coefficient β_r per unit length along the axis is calculated by Eq. (1),

$$\beta_r = \frac{192 E_{tr} I_r}{B_r^3} \tag{1}$$

where E_{tr} is the tangent modulus of the restrainer wall; I_r is the moment of inertia of the restrainer wall per unit length; and B_r is the width of the restrainer wall. The local buckling force of the core plate may then be evaluated by Eq. (2).

$$P_{crl} = 2\sqrt{\beta_r E_{tc} I_c} \tag{2}$$

where E_{tc} is the tangent modulus of the core plate; and I_c is the moment of inertia of the core plate.

In the elastic range, the buckling force derived from Eq. (2) is considerably larger than the yield strength of the core plate. However, after the yielding, the tangent modulus of the core plate E_{tc} and the spring stiffness β_r are reduced with subsequent cyclic loading. Thereafter, the local buckling force P_{crl} also decreases and local buckling failure can occur when P_{crl} becomes smaller than the core plate yield force P_{cy}. For example, the modulus characteristics of a typical BRB core plate and restrainer wall from coupon tests are depicted in Fig. 2(a) and (b). If the width of the restrainer is taken as 150 mm and the thickness of the restrainer tube is taken as either 2.3 mm or 20 mm, then the buckling force of the core plate can be obtained as shown in Fig. 2(c) and (d). For these conditions, local buckling failure is expected when the strain of the core plate exceeds approximately 2.0% and the spring stiffness of the restrainer wall decreases to 1/10 to 1/100 of its elastic range.

3. Monotonic compression tests on BRBs

To clarify the behavior and strength of BRBs consisting of a steel core plate and a mortar-filled tube restrainer, monotonic compression tests were carried out on specimens with various restrainer thicknesses. Hereafter, specimen labels are defined as RC-65; the first character represents the shape of the restrainer; *R* is rectangular shape with 1/2 scale; *Rr* is rectangular shape with 1/3 scale; *C* is a circular shape with 1/2 scale, the second character denotes the loading pattern; *C* is monotonic compression; *Y* is cyclic loading, and the third number indicates the width-to-thickness or diameter-to-thickness ratio of the restrainer steel tube. The scale of the specimens in the monotonic tests is 1/2 scale, and their details are provided in Table 1(a) and Fig. 3(a) and (c). The width-to-thickness ratios of the rectangular restrainer

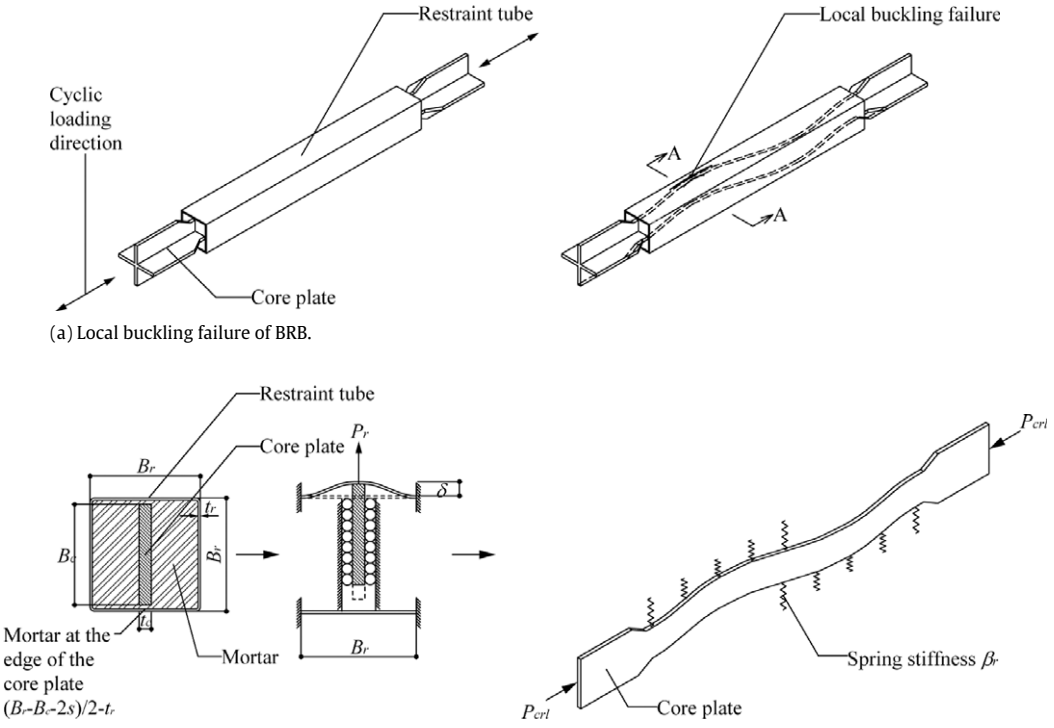

(a) Local buckling failure of BRB.

(b) Section in failure position.

(c) Core plate supported by springs.

Fig. 1. Local buckling failure of core plate in BRB.

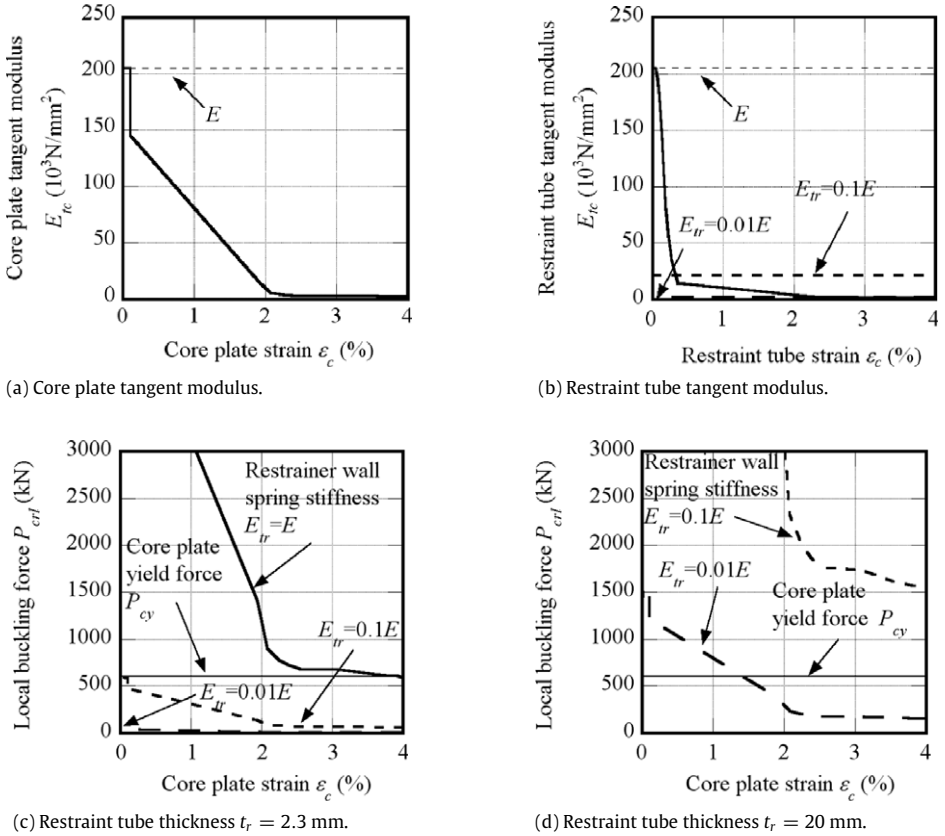

(a) Core plate tangent modulus.

(b) Restraint tube tangent modulus.

(c) Restraint tube thickness t_r = 2.3 mm.

(d) Restraint tube thickness t_r = 20 mm.

Fig. 2. Local buckling force of core plate for different restrainer wall spring stiffnesses.

are varied between 25 and 65 and the diameter-to-thickness ratio of the circular restrainer is 83. Strain gauges are attached on the surface of the restrainer along its length, oriented transversely to measure bulging due to local buckling, as shown in Fig. 3(a) (A-A view). s is the clearance between the core plate and the restrainer. To investigate the effect of mortar thickness, the size of the core plates are varied between 16 mm × 130 mm and 22 mm × 94 mm (these have the same cross-sectional areas), and

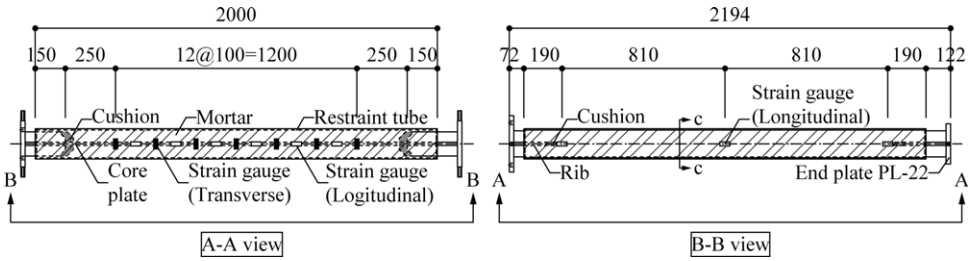

(a) Monotonic compression tests.

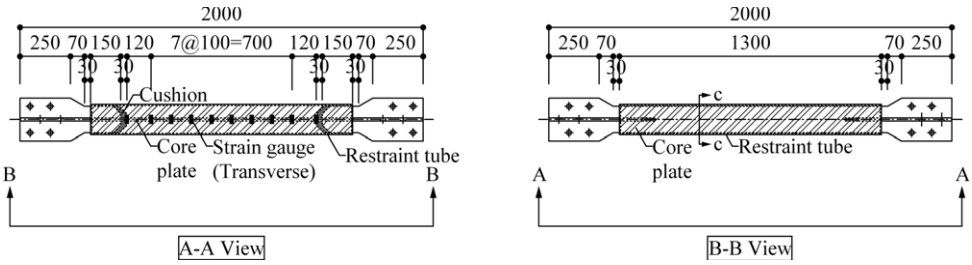

(b) Uniaxial cyclic loading tests.

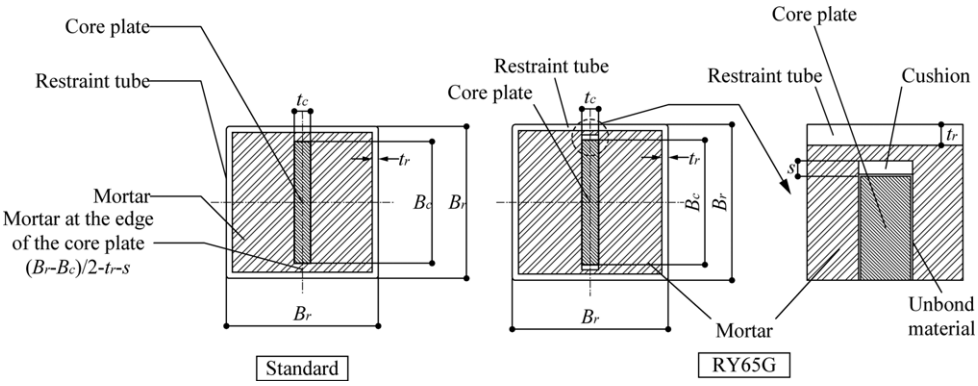

(c) c–c sectional details.

Fig. 3. Specimens for monotonic compression tests and uniaxial cyclic loading tests.

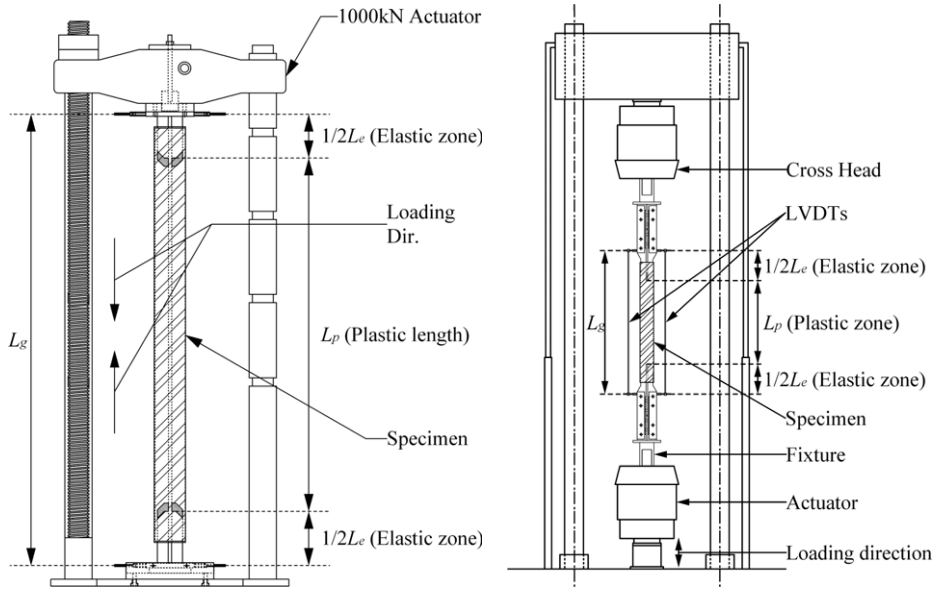

(a) Monotonic compression test. (b) Uniaxial cyclic loading test.

Fig. 4. Specimens and setup for monotonic compression and uniaxial cyclic loading tests.

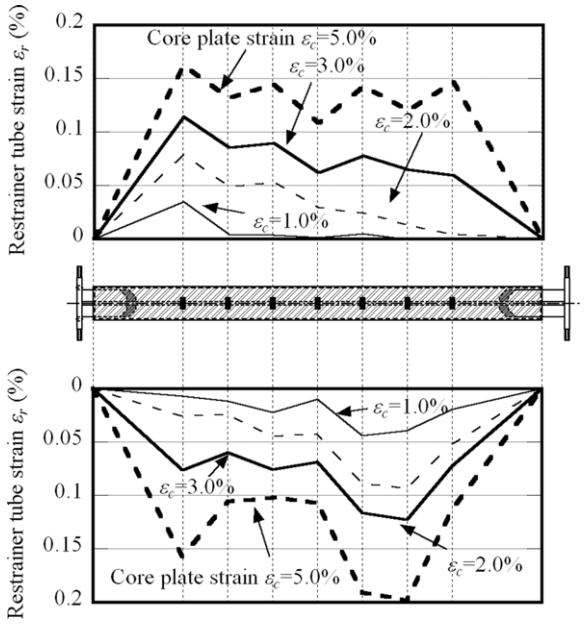

Fig. 5. Strain distribution of restrainer wall in monotonic compression test (RC65).

a monotonic compression load is applied as in Fig. 4(a). The axial force is measured by a load cell in the testing machine, and the axial displacement of the BRB is measured by extensometers between both end plates over length L_g as shown in Table 1(a) and Fig. 4(a). The displacement of the plastic zone of the core plate is defined as δ_c and is estimated by Eq. (3):

$$\delta_c = \delta_g - \frac{P_c}{A_e E} L_e \tag{3}$$

where δ_g is the extensometer displacement; P_c is the core plate axial force; A_e is the cross-section area of the core plate elastic zone; E is the elastic modulus of the core plate; and L_e is the elastic zone in the range of initial gage length. From this equation, the strain of the plastic zone of the core plate ε_c may be calculated by Eq. (4):

$$\varepsilon_c = \frac{\delta_c}{L_p}. \tag{4}$$

Strain transitions at the surface of the restrainer wall measured by the strain gauges are indicated in Fig. 5. The strain of the restrainer remained almost less than 0.1% until the core plate strain reached a strain of 3%. Consequently, no evidence of local deformation of the restrainer wall was observed. All other specimens showed similar behavior.

4. Uniaxial cyclic loading tests on BRBs

Cyclic loading tests were carried out on similar specimens to the monotonically-loaded specimens in Table 1(a). The setup of the uniaxial cyclic loading test is shown in Fig. 4(b). Both ends of the BRB are rigidly supported and a cyclic axial force is applied along its axis. The specimens are listed in Table 1(b) and shown in Fig. 3(b) and (c). The core plate is 16 mm × 130 mm for all the specimens, and in RY65G a soft cushion piece is added at the edge of the core plate to increase the clearance and to clarify the effect of the clearance on local buckling failure. The loading protocol of the test increases gradually from ±0.1%, ±0.5%, ±1%, ±2% to ±3%. Each strain has 3 cycles until ±2% strain, and ±3% strain cycle continues until the core plate fractures or the entire instability of BRBs and connections. The force applied to the BRB is measured by a load cell in the testing machine, and the axial displacement of the BRB is measured by extensometers installed between both steel end plates. The plastic strain of the core plate is evaluated by the same method as previous tests.

The hysteresis curves of core plate obtained from the test are shown in Fig. 6. Specimen RY25, with a thick restrainer wall, and Specimen CY83, with a circular restrainer, showed no local buckling failure and displayed stable stress–strain curves until the low-cycle fatigue fracture of their core plates. On the other hand, Specimens RY65 and RY65G, each having a thin restrainer wall, showed local buckling failure at 2% strain amplitude of the core plate (Fig. 7(a)). As in Fig. 6, the deterioration of the hysteresis curve occurred earlier in RY65G than in RY65. This means that the additional clearance besides the core plates leads to more significant local buckling failure. The surface strain distribution of the buckling restrainer of RY65 along with the loading is shown in Fig. 7(a). The local deformation of the restrainer wall grew significantly during the cyclic loading, and the test was stopped when the connection of the BRB became unstable due to the influence of eccentric deformation. The figure indicates that the strain in the restrainer wall increases considerably where out-of-plane deformation of the restrainer is observed. As shown in Fig. 7(b), the initial strain for the gage near the peak of the local buckle in the restrainer wall was not significant at an early stage; however, it increased dramatically once the cyclic loading achieved an amplitude of strain greater than 2%. The restrainers were disassembled after the tests and the core plates of RY25 and CY83 showed no local buckling about the strong axis, while the core plates of RY65 and RY65G showed significant wave deformation about the strong axis, with the mode depicted in Fig. 7(a). The mortar at the edge of core plate was crushed to pieces, and no contribution to the out-of-plane strength of the restrainer wall was expected.

5. Diagonal cyclic loading tests on BRBs

Cyclic loading tests were also conducted using a diagonal layout to verify the effect of bending at the ends of the BRB on its overall performance. The setup is shown as in Fig. 8. The sliding platform shown in Fig. 8 moves horizontally, and axial displacement and rotation at both ends are thus applied to the diagonal BRB specimen. The specimens have restrainer width-to-thickness ratios of 63 and 125, and the scale of the specimens is assumed to be 1/3, as shown in Table 1(c). The loading protocol of the test increases gradually from ±0.1%, ±0.5%, ±1%, ±2%, ±3%, ±4% to ±5%. Each strain has 3 cycles until ±4% strain, and ±5% strain cycle continues until the core plate fractures or the entire instability of BRBs and connections. The plastic strain of the core plate is evaluated by the same method as previous tests.

In the diagonal cyclic loading tests, local buckling failure was observed in all of the specimens, leading to overall flexural buckling after a core plate strain of 3% was reached. The mortar thickness at the edge of the core plate of Specimen RrY125M was thicker than Specimen RrY125; however, both of them showed local buckling failure. The hysteresis curve for Specimen RrY63 is shown in Fig. 9(a), and the strain transition for the gage near the peak of the local buckle in the restrainer in Specimen RrY63 is shown in Fig. 9(b). The strain of the restrainer steel wall at the local buckling area increased gradually and the local deformation was observed after the strain of the core plate exceeded 2%. This result indicates that the effect of the bending moment at the end of the BRB is not significant for the behavior of the local buckling failure because the results are similar to the uniaxial cyclic loading tests. The inner core plate of the specimens was deformed in the form of a sine wave, which was similar to that observed in the uniaxial cyclic loading tests.

Table 1
Specimen properties and test results.

Specimen	L_g (mm)	L_p (mm)	B_r (mm)	t_r (mm)	Restraint tube material	σ_{ry} (N/mm^2)	E_{tr} (N/mm^2)	B_c (mm)	t_c (mm)	Mortar thickness at the edge of core plate (mm)	σ_{cy} (N/mm^2)	E_{tc} (N/mm^2)	P_{crl} (kN) Eq. (2)	P_{cy} (kN)	P_{crl}/P_{cy}	s (mm)	Local buckling failure
(a) Monotonic compression tests																	
RC25	2172	1700	150	6.0	STKR400	436	2.05×10^5	130	16	4	258(SS400)	2.02×10^5	2.73×10^5	539	507	1.0	None
RC65				2.3	SS400	301				7.7			6.49×10^4	535	121		
RC65M					SS400		2.05×10^5	94	22	25.7				539	120		
CC83			165.2	2.0	SPHC-P	280	2.01×10^5	130	16	15.6			4.72×10^4		88		
(b) Uniaxial cyclic loading tests																	
RY25	1550	1000	150	6.0	STKR400	350	1.92×10^5	130	16	4	261(SS400)	2.05×10^5	2.66×10^5	542.9	491	1.0	None
RY65				2.3	SPHC-P	351	2.05×10^5			7.7			6.53×10^4		120	1.0	Occur
RY65G																6.0	
CY83			165.2	2.0		231	2.01×10^5			15.6			4.76×10^4		88	1.0	None
(c) Diagonal cyclic loading tests																	
RrY125	1345	920	100	0.8	SPHC-P	288	1.78×10^5	90	12	4.2	276(SS400)	2.05×10^5	9.32×10^3	297.6	31	1.0	Occur
RrY125M								68	16								
RrY63				1.6		288	2.05×10^5	90	12	3.4			2.83×10^4		95		

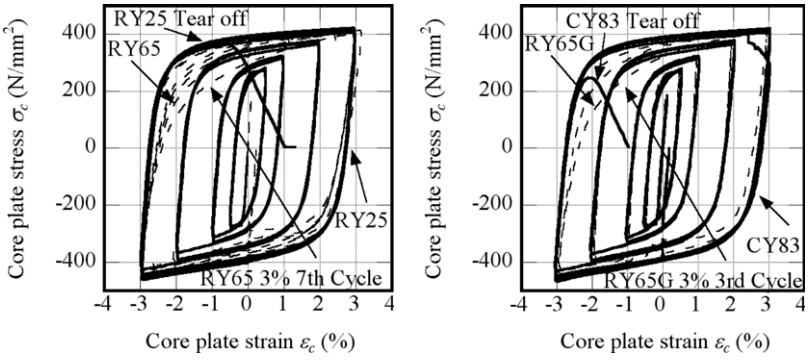

(a) RY25 and RY65. (b) CY83 and RY65G.

Fig. 6. Stress–strain curves of uniaxial cyclic loading tests.

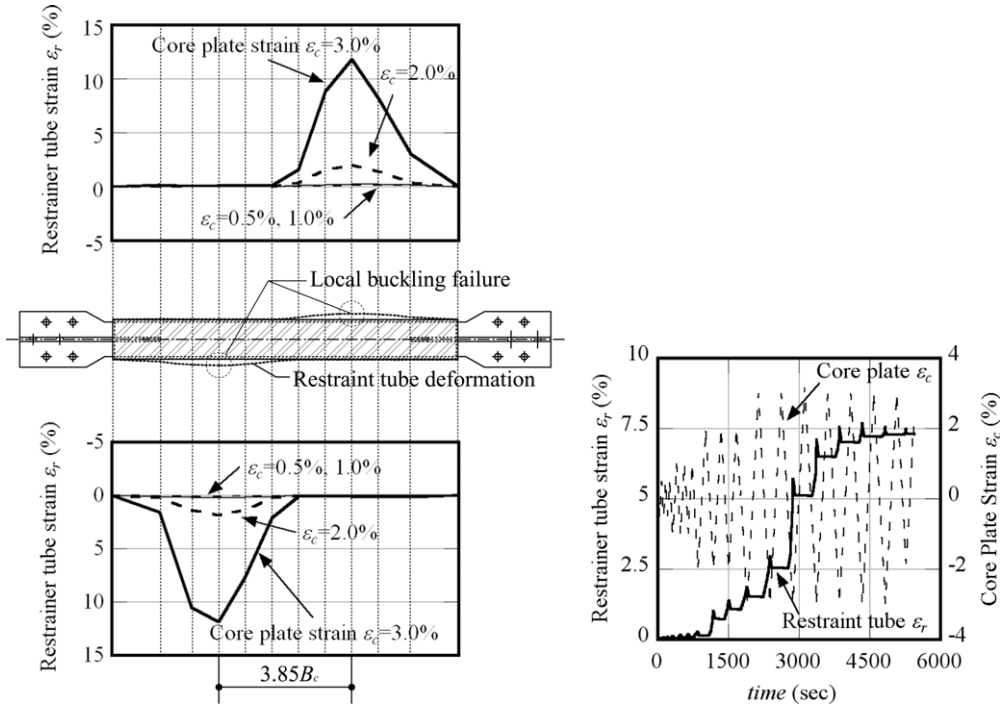

(a) Strain distribution of restrainer wall. (b) Restrainer wall strain progression.

Fig. 7. Strain distribution and progression near the peak of the local buckle in uniaxial cyclic loading test (RY65).

6. Finite element analysis of local buckling failure

To clarify the local deformation behavior of the restrainer, finite element analyses were carried out. ABAQUS (Version 6.5-6) was used for the analyses. Because the mortar was observed to have a very limited contribution to the restraint, the core plates were modeled as directly touching the restrainer walls in the analyses, as in Fig. 10(a). The deformation of the weak axis and rotation of the core plate are restrained, and initial irregularities are introduced to the core plate within the clearance between the core plate and the mortar. A shell element is used for modeling the core plate and restrainer walls, and each element had a planar aspect ratio of approximately 1. The material characteristics are modeled as in Fig. 10(b) following the RY65 coupon test results. The hardening rule was composed by the combination of isotropic and kinematic hardening as shown in Eqs. (5) and (6):

$$\sigma_{ys} = \sigma|_{ys} + \sigma_{pl} \tag{5}$$

$$\sigma_{pl} = \frac{C_1}{C_2}\left(1 - \mathrm{e}^{-C_2\varepsilon_{pl}}\right) \tag{6}$$

where σ_{ys} is the yield surface stress for isotropic hardening; $\sigma|_{ys}$ is the yield surface stress at zero plastic strain; σ_{pl} is the backstress for kinematic hardening; C_1 and C_2 are material parameters calibrated to tension coupon tests; and ε_{pl} is the plastic strain. In Fig. 11, the hysteresis curves and local strain of the restrainer obtained from the displacement-control analysis are compared with those of the cyclic loading experiment. Because the coupon test had little hardening for small plastic strains, the effect of the isotropic hardening is small in the range of the core plate strain between −2% and 2%. The test, in contrast, showed significant isotropic hardening, because of the yield plateau disappearing. However, both results generally agree, and these analyses simulate the behavior of the local buckling failure of the restrainer from the viewpoint of strain distribution. Various models changing the thickness of the restrainer wall, the clearance between the core plates and the length of the plastic zone of the core plate were prepared, and a constant cyclic load of ±3% strain was applied.

The strain progression in each case is shown in Fig. 12. The local deformation increases earlier when the restrainer was thinner, and the clearance between the core plate and the restrainer is larger. On the other hand, the length of the plastic zone of the core plate

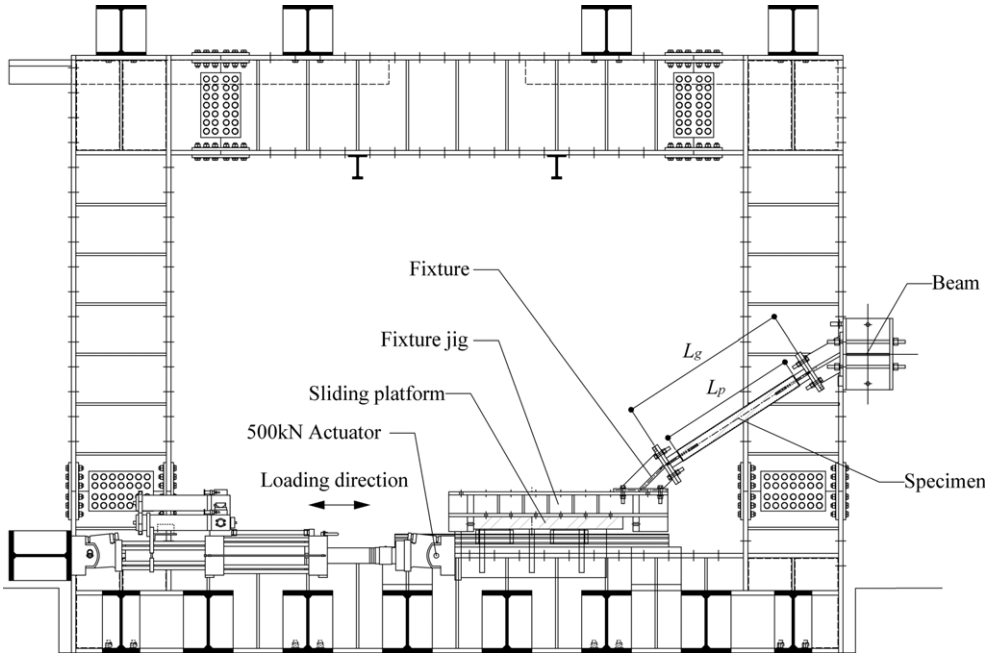

Fig. 8. Setup of diagonal cyclic loading test.

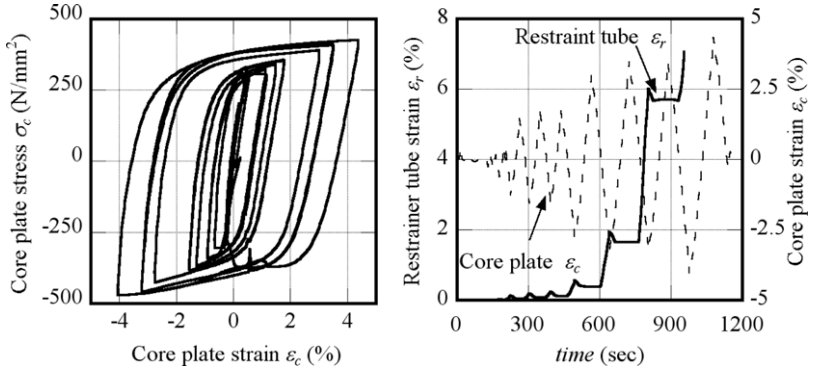

(a) Stress–strain curve. (b) Restrainer wall strain progression.

Fig. 9. Stress–strain curve and strain progression near the peak of the local buckle in diagonal loading test (RrY63).

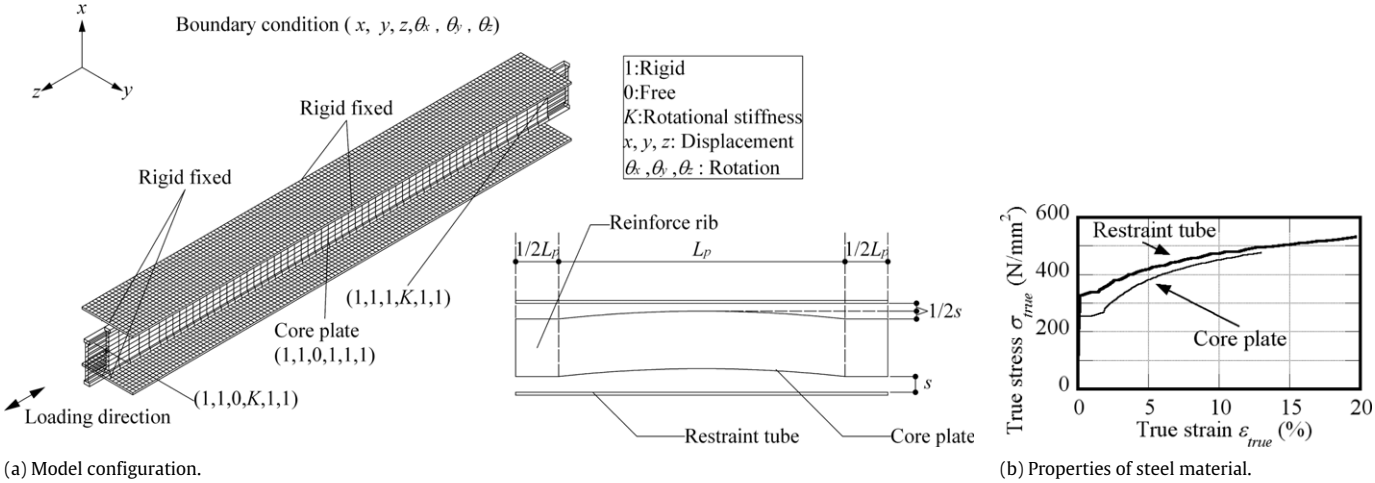

(a) Model configuration. (b) Properties of steel material.

Fig. 10. Finite element analysis model.

does not significantly affect the local deformation behavior. Also, the half length of the local buckling wave of the core plate was kept around $3.5B_c$ to $4B_c$, even when the plastic zone length of the core plate changed as shown in Fig. 13.

7. Discussion of local buckling failure criteria

Based on the results of these experiments and analyses, the length of the local buckling waves of the core plate varies ap-

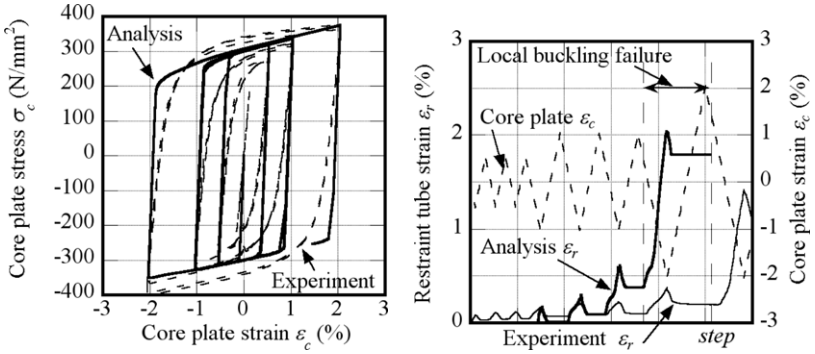

(a) Stress–strain curve. (b) Restrainer wall strain progression.

Fig. 11. Comparison between analysis and experiment (RY65).

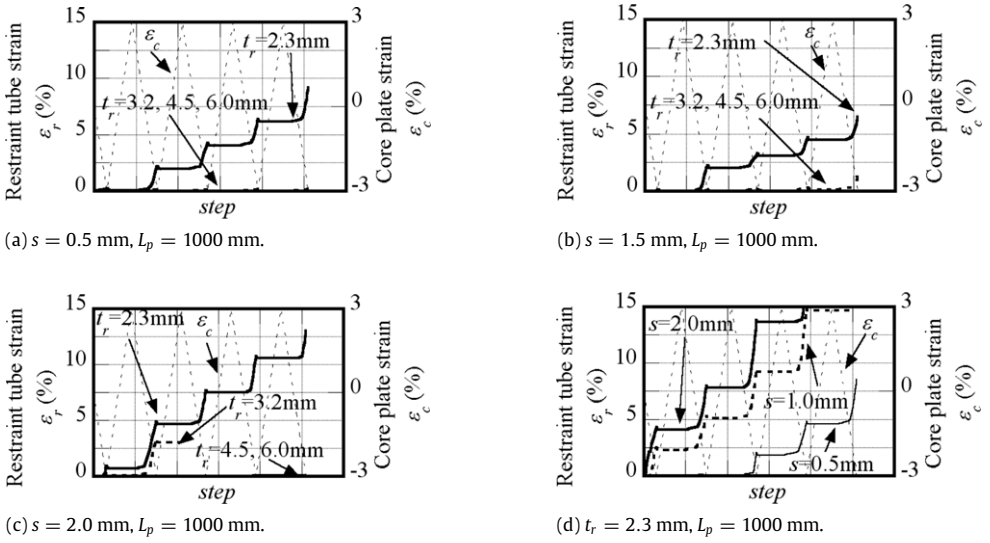

(a) $s = 0.5$ mm, $L_p = 1000$ mm. (b) $s = 1.5$ mm, $L_p = 1000$ mm.

(c) $s = 2.0$ mm, $L_p = 1000$ mm. (d) $t_r = 2.3$ mm, $L_p = 1000$ mm.

Fig. 12. Restrainer wall strain progression in various conditions.

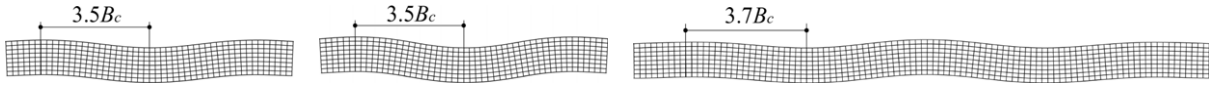

(a) $s = 0.5$ mm, $L_p = 1000$ mm. (b) $s = 2.0$ mm, $L_p = 1000$ mm. (c) $s = 0.5$ mm, $L_p = 2000$ mm.

Fig. 13. Local buckling modes in various conditions.

proximately between $3.5B_c$ to $4B_c$. The reason for this behavior is explained as follows. When the core plate buckles within the restrainer as shown in Fig. 14(a), the number of buckling wave increases with the additional axial force. However, they cease to increase at the point where the flexural buckling strength resulting from the tangent modulus of the core plate reaches the yield strength of the core plate σ_{cy}, as described by Eq. (7):

$$\sigma_{cy} = \frac{P_{cy}}{A_c} = \sigma_{cr} = \frac{\pi^2 E_{tc}}{\bar{\lambda}^2} \tag{7}$$

where A_c is the cross-section of the core plate; E_{tc} is the tangent modulus of the core plate; $\bar{\lambda} = l_p/i_c$; and i_c is the radius of gyration of the core plate. The length of the local buckling wave is then determined by Eq. (8):

$$l_p = i_c\bar{\lambda} = \frac{\pi B_c}{2}\sqrt{\frac{E_{tc}}{3\sigma_{cy}}}. \tag{8}$$

The length of local buckling wave l_p is determined by the width of the core plate and the tangent modulus in the plastic range. Where $E/\sigma_{cy} = 832$ and the tangent modulus $E_{tc} = 0.02E$, the length of the local buckling wave becomes approximately $l_p = 4B_c$. In the tensile stage, the section of the core plate decreases by $\nu_p\varepsilon_t B_c$, with the plastic Poisson's ratio $\nu_p = 0.5$. The clearance between the core plate and the restrainer increases by half of this value. The perpendicular force components working on the restrainer wall at the peak of the buckling wave can then be calculated by Eq. (9):

$$P_r = \frac{2s + \nu_p\varepsilon_t B_c}{l_p}P_{cy} = \frac{2s + \nu_p\varepsilon_t B_c}{l_p}B_c t_c \alpha\sigma_{cy} \tag{9}$$

where α is the increasing ratio of strength after yielding ($\alpha = 1.2$–1.4). From the finite element analyses, the length of the zones of the restrainer resisting against this force component is estimated to be approximately equal to the width of the restrainer as shown in Fig. 14(b). After estimating the collapse mechanism of resistance in Fig. 14(c), the perpendicular force component can be calculated by Eqs. (10) and (11):

$$M_p = \frac{B_r t_r^2}{4}\sigma_{ry} \tag{10}$$

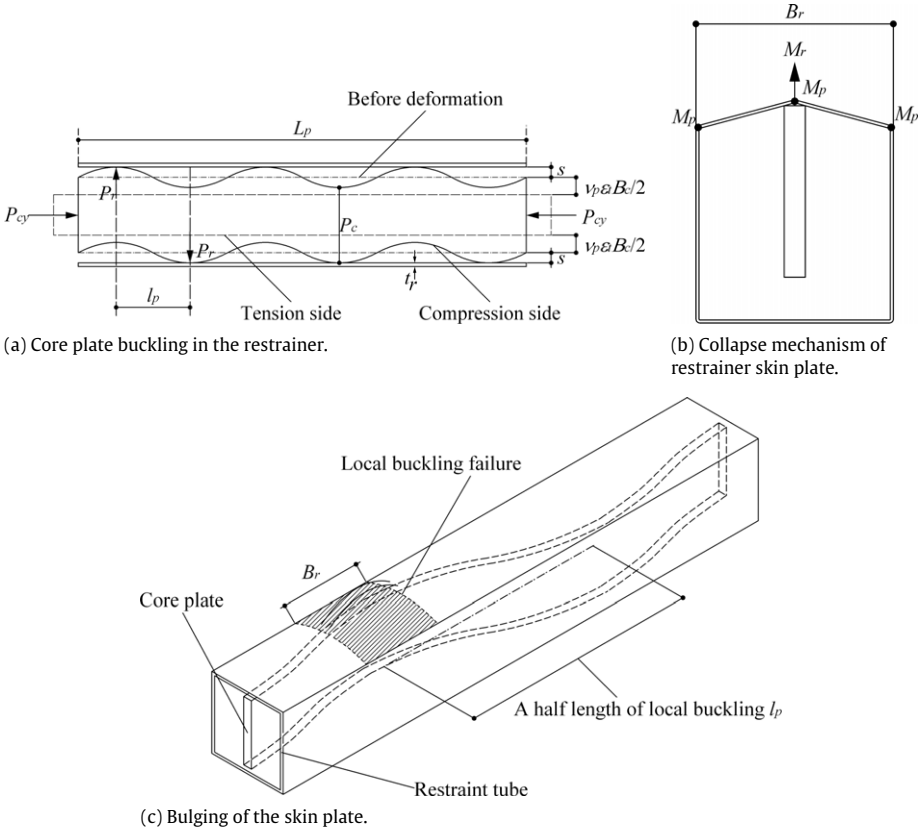

(a) Core plate buckling in the restrainer.

(b) Collapse mechanism of restrainer skin plate.

(c) Bulging of the skin plate.

Fig. 14. Collapse model of restrainer wall at local buckling failure.

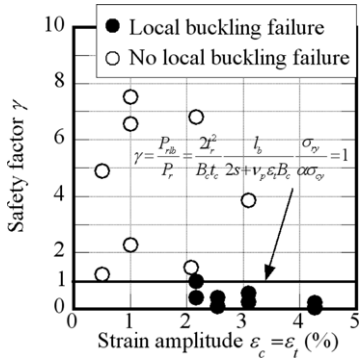

Fig. 15. Validity of proposed safety factor against local buckling failure.

$$P_{rlb} = \frac{8M_p}{B_r} = 2t_r^2\sigma_{ry}. \tag{11}$$

In these equations, σ_{ry} is the yield stress of the restrainer wall. The ratio γ is then defined by Eq. (12) as the ultimate strength of the restrainer wall P_{rlb} divided by the perpendicular force component of the core plate P_r:

$$\gamma = \frac{P_{rlb}}{P_r} = \frac{2t_r^2}{B_c t_c}\frac{l_p}{2s+\nu_p\varepsilon_t B_c}\frac{\sigma_{ry}}{\alpha\sigma_{cy}}. \tag{12}$$

In this equation, ε_t is the expected maximum tensile strain of the core plate, which is estimated as 0 for the simple compression test. The ratio γ represents the safety factor against local buckling failure, and the axial force P_{lb} causing the local buckling failure can be calculated by Eqs. (13) and (14) as follows:

$$P_{lb} = 2t_r^2\frac{l_p}{2s+\nu_p\varepsilon_t B_c}\sigma_{ry} \tag{13}$$

$$\gamma = \frac{P_{lb}}{\alpha P_{cy}}. \tag{14}$$

The γ indices estimated from the test specimens are shown in Fig. 15 together with the occurrence of local buckling failure. From this figure, it is observed that all specimens with γ less than 1.0 caused local buckling failure, and the criteria for the restrainer wall are well explained by this index. Although the results of the circular restrainer are not included in this assessment, the limited results indicate that judging with the γ index leads to a safer design.

8. Conclusions

In this study, experiments and numerical analyses were carried out using buckling restrained brace members that consist of steel core plates and mortar-filled steel tube restrainers. The phenomenon of local buckling failure encountered in these specimens was investigated to assess its influence on the strength and ductility of the BRBs. As a result, the following conclusions were obtained:

(1) When the restrainer steel tube is assumed to be an elastic spring, no local buckling failure of restrainer tube is expected. However, when the tangent modulus of the core plate and the restrainer wall are decreased in the plastic range, the possibility of local buckling failure increases.
(2) Monotonic compression tests on BRBs with thinner restrainers were carried out; however, no specimen showed local buckling failure up to a core plate strain of 5%.
(3) Uniaxial cyclic loading tests were carried out on the similar specimens to monotonic compression tests, and local buckling failures were observed in specimens possessing rectangular tubes with a width-to-thickness ratio of 65. A significant increase in the strain on the restrainer wall was observed

during cyclic loading. On the other hand, specimens containing a rectangular tube with a width-to-thickness ratio of 25, and a circular tube with a diameter-to-thickness ratio of 83 did not show evidence of local buckling failure.

(4) Diagonal cyclic loading tests were also conducted with the diagonal layout being comparable to an actual building, and local buckling failures were observed in all specimens possessing rectangular tubes with a diameter-to-thickness ratio of 63 or 125. A significant increase in the strain on the restrainer wall was observed during cyclic loading. The results of this test were similar to those of the uniaxial cyclic loading tests, so the bending at the end connections did not have much influence on the occurrence of local buckling failures.

(5) From nonlinear finite element analyses that were conducted through modeling the BRBs with a series of shell elements, the increase of strain in the restrainer wall become more significant with a thinner restrainer wall and a larger clearance between the edge of the core plate and the restrainer. On the other hand, the length of the core plate does not affect the local buckling behavior, and local buckling wave lengths are kept in a range of approximately 3.5 to 4.0 times the core plate width.

(6) The local buckling wave length of the core plate can be well explained by a slenderness ratio calculated by buckling strength using the tangent modulus and maximum yield force of core plate. Considering the restrainer wall and the maximum tensile strain of the core plate, a criterion for local buckling restraint failure is provided. The proposed index agrees well with the results of the experiments, and it is considered to be valid for practical design of BRBs.

Acknowledgements

This research was supported by Nippon Steel Engineering Co., Ltd. and the University of Illinois at Urbana-Champaign. The authors thank Matthew Eatherton, Grzegorz Banas, and Timothy Prunkard of the University of Illinois at Urbana-Champaign for their contributions to the experiments conducted in this research. Any opinions, findings, and conclusions or recommendations expressed in this material are those of the authors and do not necessarily reflect the views of the sponsors.

References

[1] Watanabe A, Hitomi Y, Saeki E, Wada A, Fujimoto M. Properties of brace encased in buckling-restraining concrete and steel tube. In: Proc., 9th conference on earthquake engineering. vol. IV; 1988. p. 719–24.

[2] Qiang X. State of the art of buckling-restrained braces in Asia. Journal of Constructional Steel Research 2005;61:727–48.

[3] Clark P, Aiken I, Kasai K, Ko E, Kimura I. Design procedures for buildings incorporating hysteretic damping devices. In: Proc., 69th annual convention. SEAOC; 1999. p. 355–71.

[4] Black CJ, Makris N, Aiken ID. Component testing and modeling of buckling restrained unbonded braces. In: Proc., STESSA; 2003.

[5] Black CJ, Makris N, Aiken ID. Component testing, seismic evaluation and characterization of buckling-restrained braces. Journal of the Structural Engineering, ASCE 2004;130(6):880–94.

[6] Sabelli R, Mahin S, Chang C. Seismic demands on steel braced frame buildings with buckling-restrained braces. Engineering Structures 2003;5:655–66.

[7] Fahnestock LA, Sause R, Ricles JM. Seismic response and performance of buckling-restrained braced frames. Journal of the Structural Engineering, ASCE 2007;133(9):1195–204.

[8] Fahnestock LA, Ricles JM, Sause R. Experimental evaluation of a large-scale buckling-restrained brace frame. Journal of the Structural Engineering, ASCE 2007;133(9):1205–14.

[9] Takeuchi T, Suzuki K, Marukawa T, Kimura Y, Ogawa T, Sugiyama T, et al. Performance of compressive tube members with buckling restrained composed of mortar in-filled steel tube. Journal of Structure and Construction Engineering, AIJ 2005;590:71–8. [in Japanese].

[10] Takeuchi T, Yamada S, Kitagawa M, Suzuki K, Wada A. Stability of buckling-restrained braces affected by the out-of-plane stiffness of the joint element. Journal of Structure and Construction Engineering, AIJ 2004;575:121–8. [in Japanese].

[11] Tsai KC, Hsiao PC, Wang KJ, Weng YT, Lin ML, Lin KC, Chen CH, et al. Pseudo-dynamic tests of a full scale CFT/BRB frame-Part :Specimen design, experiment and analysis. Earthquake Engineering and Structural Dynamics 2008;37:1081–98.

[12] Kinoshita T, Koetaka Y, Inoue K, Iitani K. Out-of-plane stiffness and yield strength of cruciform connection for buckling-restrained brace. Journal of Structure and Construction Engineering, AIJ 2008;632:1865–73. [in Japanese].

[13] Tembata H, Koetaka Y, Inoue K. Out-of-plane buckling load of buckling restrained braces including brace joints. Journal of Structure and Construction Engineering, AIJ 2004;581:127–34. [in Japanese].

[14] Kinoshita T, Koetaka Y, Inoue K, Iitani K. Criteria of buckling-restrained braces to prevent out-of-plane buckling. Journal of Structure and Construction Engineering, AIJ 2007;621:141–8. [in Japanese].

[15] Iwata M, Murase R, Izumita Y, Murai M. Experimental study on buckling-restrained braces using steel mortar planks -Part 3 Buckling behavior of core plate. Journal of Structure and Construction Engineering, AIJ 2007;611:133–9. [in Japanese].